

**EXPLAINING AND FORECASTING INTERANNUAL VARIABILITY IN
THE FLOW OF THE NILE RIVER**

Mohamed S. Siam¹

Ralph M. Parsons Laboratory, Massachusetts Institute of Technology, Cambridge,
Massachusetts

Elfatih A. B. Eltahir

Ralph M. Parsons Laboratory, Massachusetts Institute of Technology, Cambridge,
Massachusetts

¹*Corresponding author address:* Mohamed Siam, Ralph M. Parsons Laboratory, Massachusetts
Institute of Technology, 15 Vassar St. Cambridge, MA 02139.
E-mail:msiam@mit.edu

1 **EXPLAINING AND FORECASTING INTERANNUAL VARIABILITY IN**
2 **THE FLOW OF THE NILE RIVER**

3
4 **Abstract**

5
6 This study analyzes extensive data sets collected during the 20th century and define four modes of
7 natural variability in the flow of Nile River, identifying a new significant potential for improving
8 predictability of floods and droughts. Previous studies have identified a significant teleconnection
9 between the Nile flow and the Eastern Pacific Ocean. El Niño-Southern Oscillation (ENSO)
10 explains about 25% of the interannual variability in the Nile flow. Here, this study identifies a
11 region in the southern Indian Ocean with similarly strong teleconnection to the Nile flow. Sea
12 Surface Temperature (SST) in the region (50°E-80°E and 25°S-35°S) explains 28% of the
13 interannual variability in the flow of Nile river and when combined with **ENSO index the explained**
14 **variability of the flow of Nile river increases to 44%**. In addition, during those years with
15 anomalous SST conditions in both Oceans, this study estimates that indices of the SSTs in the
16 Pacific and Indian Oceans can collectively explain up to 84% of the interannual variability in the
17 flow of Nile. Building on these findings, this study uses classical Bayesian theorem to develop a
18 new hybrid forecasting algorithm that predicts the Nile flow based on global models predictions
19 of indices of the SST in the Eastern Pacific and Southern Indian Oceans.

22 1. Introduction

23 The Nile basin covers an area of 2.9×10^6 km², which is approximately 10% of the African
24 continent (Fig. 1). It has two main tributaries; the White Nile and the Blue Nile that originate from
25 the equatorial lakes and Ethiopian highlands respectively. The Upper Blue Nile (UBN) basin is
26 the main source of water for the Nile River. It contributes to approximately 60% of the annual flow
27 of the Nile and 80% of the total Nile flow that occurs between July and October at Dongola
28 (Conway and Hulme, 1993) (Fig. 2). The UBN basin extends over an area of 175×10^3 km² (7° N
29 to 12°5' N and from 34°5' E to 40° E). The mean annual rainfall over this basin is 1200 mm/year
30 (Conway and Hulme, 1993). Almost 60% of the annual rainfall over the UBN occurs during the
31 summer between July and August, resulting in a largely predictable seasonal variability in the flow
32 of the river.

33

34 The prediction of inter-annual variability in the flow of the Nile is rather challenging. Many studies
35 investigated the teleconnections between the Ethiopian rainfall and the global Sea Surface
36 Temperature (SSTs) in order to find SSTs indices to use for Nile flow prediction (e.g. Eltahir,
37 1996; Abteu et al., 2009; and Melesse et al., 2011). Eltahir (1996) showed that the SSTs anomalies
38 over the tropical Eastern Pacific Ocean explains 25% of the inter-annual variability of Nile flow
39 for the period 1872-1972. ElSanabary et al., 2014 showed that the dominant frequencies of the
40 Ethiopian rainfall ranged between 2 and 8 years and that the scale averaged wavelet power of the
41 SSTs over the Eastern Pacific and South Indian and Atlantic Oceans can explain significant
42 fraction of the rainfall variability over Ethiopia using wavelet principal component analysis. These
43 correlations between the Nile flow and SSTs indices were the basis for new forecast models that
44 were proposed to predict the Nile flows. For example, Wang and Eltahir (1999) used a discriminant

45 prediction approach to estimate the probabilities that the Nile flow will fall into prescribed
46 categories. Eldaw et al., (2003) and Gissila et al., (2004) used sea surface temperature (SST) over
47 the Pacific, Indian and Atlantic Oceans as predictors within a multiple linear regression model to
48 predict the Nile flow.

49

50 The mechanisms behind these teleconnections between the rainfall over Ethiopia and the global
51 SSTs were examined in several studies (e.g. Beltrando and Camperlin, 1993). However, a clear
52 distinction must be made between rainfall over the UBN basin in Ethiopia and rainfall over East
53 Africa, defined as the region along the coast, east of the Ethiopian highlands (Fig. 1). The UBN
54 basin has one rainy season (May to September) during which more than 80% of the rainfall occurs,
55 while along the East coast of Africa and depending on the location from the equator, the seasonal
56 cycle of rainfall can have two rainy seasons (Black et al., 2003, Hastenrath et al., 2011). This
57 pattern in the seasonal cycle of rainfall is related to the migration of the Inter-tropical Convergence
58 Zone (ITCZ) across the equator. Camberlin, 1995 showed that the rainfall over East Africa,
59 including the UBN basin, is strongly coupled with the dynamics of the Indian monsoon. During
60 strong Indian monsoon seasons, the sea level pressure over India decreases significantly, which
61 enhances the pressure gradient between East Africa and India. **As a result, westerly winds increase**
62 **over Eastern Africa and enhance transport moisture from the Congo basin to Ethiopia, Uganda and**
63 **western Kenya.** Giro et al., 2010 also showed that the warming over the Pacific Ocean, during El
64 Niño events, reduces these westerly winds, which reduce the rainfall over East Africa. In addition,
65 the monsoon circulation is weaker during El Niño events due to modulation of the walker
66 circulation and enhanced subsidence over the Western Pacific and South Asia, thus the rainfall
67 over Ethiopia decreases (Ju and Slingo, 1995; Kawamura, 1998; Shukla and Wallace, 1983; Soman

68 and Slingo, 1997). The reduced Nile flows during El Niño events were also attributed to the
69 enhanced tropical-scale subsidence that suppresses rainfall, as a consequence of the increased
70 upwelling over the Eastern Pacific Ocean (Amarasekera et al., 1996).

71

72 The physical mechanism of the teleconnection between the Nile flow and SSTs of North and
73 Middle Indian Ocean and ENSO is described in another paper by the authors (Siam et al., 2014).
74 Nile flow is strongly modulated by ENSO through ocean currents. During El Niño events, the
75 warm water travels from the Pacific to the Indian Ocean through the “Indonesian through flow”
76 and advection by the Indian Equatorial Current (Tomczak and Godfrey, 1995). As a result, SSTs
77 in North and Middle Indian Ocean warm-up following the warming of Tropical Eastern Pacific,
78 and forces a Gill type circulation anomaly with enhanced westerly winds over Western Indian
79 Ocean (Yang et al., 2007). The latter enhances the low-level divergence of air and moisture away
80 from the Upper Blue Nile resulting in a reduction of rainfall over the basin. **On the other hand, the**
81 **warming over the South Indian Ocean, generates a cyclonic flow in the boundary layer, which**
82 **reduces the cross-equatorial meridional transport of air and moisture towards the UBN basin,**
83 **favoring a reduction in rainfall and river flows.** The tele-connections between the Pacific Ocean
84 and the Nile basin and between the Indian Ocean and the Nile basin are reflected in different modes
85 of observed natural variability in the flow of Nile River, with important implications for the
86 predictability of floods and droughts.

87

88 The objectives of the study are (i) to investigate the **strength of the** teleconnection between the
89 Indian Ocean and the Nile basin and its role in explaining observed natural modes of variability in
90 the flow of the Nile river, and (ii) to develop a new hybrid forecasting algorithm that can be used

91 to predict the Nile flow based on indices of the SST in the Eastern Pacific and Southern Indian
92 Oceans.

93

94 **2. Data**

95 In this study we use observed SSTs over the Indian and Pacific oceans from the monthly global
96 (HadISST V1.1) dataset on a 1 degree latitude-longitude grid from 1900 to 2000 (Rayner et al.
97 2003). The monthly flows at Dongola from 1900 to 1984 were extracted from the Global River
98 Discharge Database (RivDIS v1.1) (Vörösmarty et al., 1998) and from 1984 to 2000 through
99 personal connection. The average monthly anomalies from September to November of the SSTs
100 averaged over the Eastern Pacific Ocean (6°N-2°N, 170°W-90°W; 2°N-6°S, 180°W-90°W; and
101 6°S-10°S, 150°W-110°W) are used as an index of ENSO. This area has shown the highest
102 correlation with the Nile flows and it is almost covering the same area as Niño 3 and 3.4 indices
103 (Trenberth, 1997).

104

105 **3. Relation between the variability in the flow of Nile river, ENSO and the Indian Ocean SST**

106 Based on extensive correlation analysis of the Nile river flow at Dongola and the observed SST in
107 the Indian Ocean, this study identifies a region over the Southern Indian Ocean (50°E-80°E and
108 25°S-35°S) (see Figure 3) as the one with the highest correlation between SST and the Nile flow.
109 This correlation is especially high for river flow (accumulated for July, August, September and
110 October) and SST during the month of August. **An earlier study by ElDaw et al. (2003)** used SST
111 indices over the Indian Ocean to predict the Nile flow, however, they focused on regions of the

112 Indian Ocean that are different from the region that we use in defining the **South Indian Ocean**
113 **(SIO)** index. In other words the region of the SIO was not used by EIDaw et al. (2003). Table 2
114 describes the regions of the Indian Ocean identified in both studies.

115
116 This study emphasizes that the proposed forecasting methodology for the Nile flow is motivated
117 by the physical mechanisms proposed by Siam et al. (2014) and described in Section 1. **In contrast,**
118 the forecasting approach of some of the previous studies was based on purely statistical
119 correlations found between the Nile flow and SSTs globally.

120
121 Figure 4 shows the observed and simulated time series of the average July to October Nile flow at
122 Dongola, which accounts for approximately 70% of the annual Nile flow. The Nile flow is
123 **predicted by three different linear regression models using either ENSO averaged from September**
124 **to November (Figure 4a) or SIO August (Figure 4b) indices, or both (Figure 4c) as covariates. It**
125 **is clear from this figure that the addition of the SIO index increase the explained variability of the**
126 **Nile flow to 44%, compared to only 30% when ENSO index is used alone. This indicates that the**
127 **SIO index can explain almost 14% of the variability of the Nile flow that is independent from**
128 **ENSO.** The North and middle of the Indian Ocean have also exhibited a high correlation between
129 their SST and the Nile flow. However, the additional variability explained by the SST over the
130 North and Middle Indian Ocean, when combined with the ENSO index, is negligible (not shown
131 here). This is mainly because the SSTs over the North and Middle Indian Ocean are dependent on
132 ENSO, while the SSTs over the South Indian Ocean (i.e. SIO index) is not, as described in Section
133 1.

134

135 In further analysis, we define $\pm 0.5^{\circ}\text{C}$ as the threshold between non-neutral and neutral years on the
136 Eastern Pacific Ocean based on ENSO index. This value is about two-thirds of one standard
137 deviation of the anomalies of ENSO index. The same threshold has been used to identify non-
138 neutral and neutral years using El Niño 3.4 index, which is similar to our ENSO index (Trenberth,
139 1997). This indicates that if the ENSO index anomaly is greater than 0.5°C or less than -0.5°C , it
140 is considered as non-neutral condition, otherwise, it is considered as neutral condition. Similarly,
141 $\pm 0.3^{\circ}\text{C}$ value is used as a threshold between non-neutral and neutral years on the South Indian
142 Ocean using the SIO index. This value is also about two-thirds of one standard deviation for the
143 anomalies of the SSTs over this region. Thus, if both ENSO and SIO indices are used together,
144 four different combinations can be defined based on these classifications. The first is when both
145 ENSO and SIO indices are neutral (29 out of 100 events), the second is when both ENSO and SIO
146 indices are non-neutral (19 out of 100 events), the third when SIO is non-neutral and ENSO is
147 neutral (26 out of 100 events) and finally when SIO is neutral and ENSO is non-neutral (26 out of
148 100 events). Each of these combinations is considered as a mode of natural variability in the flow
149 of Nile river. Then the Nile flow is calculated as a predictant using multiple linear regression with
150 the (ENSO and SIO indices) of each mode as predictors.

151

152 Four different modes are identified for describing the natural variability in the flow of Nile River
153 and summarized in (Table 1). The ENSO and SIO indices do not explain a significant fraction of
154 the interannual variability in the flow of river when they are both neutral (Fig. 5a). The variability
155 of the Nile flow in such years can be regarded as a reflection of the chaotic interactions between
156 the biosphere and atmosphere and within each of the two domains. For this mode, the predictability
157 of the Nile flow is rather limited. The other two intermediate modes include non-neutral conditions

158 in the Eastern Pacific and neutral conditions in the Southern Indian Oceans or vice versa (Fig. 5b
159 and 5c). For these two modes, a significant fraction (i.e. 31% and 43%) of the variance describing
160 inter-annual variability in the flow is explained. Hence, these modes point to a significant potential
161 for predictability of the flow. Finally, indices of ENSO and SIO can explain 84% of the interannual
162 variability in the Nile flow when non-neutral conditions are observed for both the Eastern Pacific
163 and Southern Indian Oceans (Fig. 5d). Therefore, the SIO index can be used to predict the flow
164 together with the ENSO index, as collectively they can explain a significant fraction of the
165 variability in the flow of Nile River. This result indicates that during years with anomalous SST
166 conditions in both oceans, floods and droughts in the Nile River flow can be highly predictable,
167 assuming accurate forecasts of those indices are available.

168

169 **4. A Hybrid Methodology for Long-range Prediction of the Nile flow**

170 A simple methodology is proposed to predict the Nile flow with a lead time of about a few months
171 (~3-6 months). The forecast of global SST distribution based on dynamical models (e.g. NCEP
172 coupled forecast system model version 2 (CFSv2), Saha et al., 2010; Saha et al., under review),
173 can be used together with the algorithm developed in this section to relate the Nile flow to ENSO
174 and SIO indices. The proposed method is shown in Figure 6 and can be described in two main
175 steps:

- 176 • Forecast of SST anomalies in the Indian Ocean and Eastern Pacific Ocean using dynamical
177 models of the coupled global ocean atmosphere system. Such forecasts are routinely issued by
178 centers such NCEP and ECMWF.

179 • Application of a forecast algorithm between the Nile flow (predictand) and forecasted SSTs
180 in the Indian and Eastern Pacific Oceans (predictors) for the identified mode of variability.

181
182 In this paper we focus on the second step of the proposed method: the development of the algorithm
183 relating SSTs and the Nile flow. We develop the forecast algorithm using observed SSTs. We do
184 not describe how this algorithm can be applied with forecasts of global SST distribution based on
185 dynamical models as this step is beyond the scope of this paper. However, we recognize that
186 overall accuracy of this method in predicting interannual variability of the Nile flow is dependent
187 on the skill of global coupled models in forecasting the global SSTs (See Appendix for information
188 about forecasting models). Thus, the selection of the forecast model, which predicts the SSTs is
189 an important step to ensure the accuracy of the prediction of the Nile flow. As global coupled
190 ocean-atmosphere models improve in their skill of forecasting global SSTs in the Pacific and
191 Indian Oceans, we expect that our ability to predict the interannual variability in the Nile flow will
192 improve too. In addition, the accuracy in the prediction of the Nile flow at medium and short time
193 scales (of weeks to one month) can be improved by adding other hydrological variables (e.g.
194 rainfall and stream flow) over the basin, as demonstrated by (Wang and Eltahir, 1999)

195 The proposed method can be described as hybrid since it combines dynamical forecasts of global
196 SSTs, and statistical algorithms relating the Nile flow and the forecasted SSTs. The same method
197 can also be described as hybrid since it combines information about SSTs from the Pacific and the
198 Indian Oceans.

199 Here, we apply a discriminant approach that specifies the categoric probabilities of the predictand
200 (Nile flow) according to the categories that the predictors (i.e. ENSO and SIO indices) fall into.

201 The annual Nile flow is divided into “low”, “normal”, and “high” categories. The boundaries of
 202 these categories are defined so that the number of points in each category is about a third of the
 203 data points (Fig 7). On the other hand, the ENSO and SIO indices are divided into “cold”, “normal”
 204 and “warm” categories. (The words Normal and Neutral are used to describe the same
 205 conditions).The boundaries for the normal category are -0.5°C and 0.5°C for ENSO index and -
 206 0.3°C and 0.3°C for SIO index (Fig. 7). Any condition below the lower limit is considered “cold”
 207 and higher than the upper limit is considered “warm” for both indices.

208 The Bayesian theorem, described in many statistical books (e.g., Winkler 1972; West 1989), states
 209 that the probability of occurrence of a specified flow category (Q_i) and given two conditions (A
 210 and B) can be expressed as

$$211 \quad P(Q_i/ A, B) = \frac{P(B/Q_i, A)P(Q_i/A)}{P(B/A)} \quad (1)$$

212 Where $P(Q_i/ A)$ is the probability of event Q_i given that event A has occurred, and $P(Q_i/ A, B)$ is
 213 the probability of event Q_i given that events A and B have occurred, and similarly for other shown
 214 probabilities. In addition, if the events A and B are independent, we can rewrite Eq. (1) as

$$215 \quad P(Q_i/ A, B) = \frac{P(B/Q_i)P(Q_i/A)}{\sum_{i=1}^3 P(B/Q_i)P(Q_i/A)} \quad (2)$$

216 The advantage of assuming independence between (A and B) and using Eq. (2), it simplifies the
 217 calculation of $P(B/Q_i, A)$ since we do not have to split the data into a relatively large number of
 218 categories, which reduces the error due to the limitation of the data size. The independence
 219 between ENSO and SIO indices is a reasonable assumption as the coefficient of determination
 220 between them is less than 6%.

221

222 In order to evaluate the predictions of the Nile flow, we use a forecasting index (FI) defined by
223 Wang and Eltahir, (1999) as

$$224 \quad FP(j) = \sum_{i=1}^3 P_r(i, j) P_p(i, j) \quad (3)$$

$$225 \quad FI = \frac{1}{n} \sum_{i=1}^n FP(j) \quad (4)$$

226 Where $FP(j)$ is the forecast probability in a certain year (j) and the FI is the average of the FP over
227 a certain period, n . The prior probability $P_r(i, j)$ is calculated using Eq.(2) for a certain year (j) and
228 category ($i=1, 2, 3$) and the posterior probability $P_p(i, j)$ is defined as [1,0,0] in low flow year,
229 [0,1,0] in normal year, and [0,0,1] in a high flow year. Hence, a larger FI indicates a higher
230 accuracy of the forecast. The FI without any information about SST, should be about one third as
231 we have classified flow data into three categories each with a similar number of the data points.

232 The data is split into a calibration period (1900-1970) and a verification period (1970-2000).
233 Tables 3 and 4 summarize the conditional probabilities of Nile flow given certain conditions of
234 SIO or ENSO index. It is shown that during “warm” and “cold” conditions of SIO, the probabilities
235 are significantly higher for “low” and “high” Nile flow, respectively. The same is true for the
236 ENSO, as was described originally by Eltahir (1996). Table 5 shows the probabilities that are
237 conditioned on both SIO and ENSO, calculated using Eq. (2). This table illustrates clearly how
238 forecasts of the Nile flow can be improved by combining the two indices. For example, “warm”
239 conditions in both oceans translate into 85% probability of “low” flow in the Nile, and insignificant
240 probability of “high” flow. On the other hand, “cold” conditions in both oceans translate into 83%
241 probability of “high” flow in the Nile, and insignificant probability of “low” flow. Depending on
242 the accuracy of the dynamical forecast models of global SSTs, such forecast of the Nile flow can
243 be issued with lead times of 6 months. At present, the Eastern Nile Regional technical Office

244 (ENTRO) issues operational forecasts of the Nile flow based on ENSO forecasts and the
245 probability table described by Eltahir (1996) (similar to Table 4). We anticipate that use of Table
246 5, would represent a significant improvement in these operational forecasts.

247 The combined use of ENSO and the SIO indices significantly increased the FI to 0.5 (Figure 8a).
248 Comparison of Figures 8b and 8c, illustrates that the SIO index alone has almost the same FI value
249 as ENSO index. Recall that in absence of any information about global SSTs, the FI should have
250 a value of one third. The deviations of the FI using ENSO index alone (Figure 8b) or SIO index
251 alone (Figure 8c) from one third are almost added together to create the deviation of the FI from
252 the hybrid method from one third (Figure 8a). Hence, the new SIO index plays an independent role
253 from ENSO in shaping the interannual variability in the flow of Nile River. Thus by using these
254 two indices, we explain a significant fraction of the interannual variability in the flow of Nile
255 River, and illustrate a significant potential for improving the Nile flow forecasts.

256 **5. Conclusions**

- 257 • In this paper, we document that the SSTs in the Eastern Pacific and Indian Oceans play a
258 significant role in shaping the natural interannual variability in the flow of Nile River.
259 Previous studies have identified a significant teleconnection between the Nile flow and the
260 Eastern Pacific Ocean. El Niño-Southern Oscillation (ENSO) explains about 25% of the
261 interannual variability in the Nile flow. Here, this study identifies a region in the southern
262 Indian Ocean with similarly strong teleconnection to the Nile flow. Sea Surface
263 Temperature (SST) in the region (50°E-80°E and 25°S-35°S) explains 28% of the
264 interannual variability in the Nile flow.
- 265 • In addition, four different modes of natural variability in the Nile flow are identified and it
266 is shown that during non-neutral conditions in both the Pacific and Indian Oceans, the Nile

267 flow is highly predictable using global SST information. During those years with
268 anomalous SST conditions in both Oceans, this study estimates that indices of the SSTs in
269 the Pacific and Indian Oceans can collectively explain up to 84% of the interannual
270 variability in the flow of Nile. The estimated relationships between the Nile flow and these
271 indices allow for accurately predicting the Nile floods and droughts using observed or
272 forecasted conditions of the SSTs in the two oceans.

- 273 • This study uses classical Bayesian theorem to develop a new hybrid forecasting algorithm
274 that predicts the Nile flow based on indices of the SST in the Eastern Pacific and Southern
275 Indian Oceans. “Warm” conditions in both oceans translate into 85% probability of “low”
276 flow in the Nile, and insignificant probability of “high” flow. On the other hand, “cold”
277 conditions in both oceans translate into 83% probability of “high” flow in the Nile, and
278 insignificant probability of “low” flow. Applications of the proposed hybrid forecast
279 method should improve predictions of the interannual variability in the Nile flow, adding
280 a new a tool for better management of the water resources of the Nile basin.

281 The proposed forecasting methodology is indeed dependent on the accuracy of the global SST
282 forecasts from global dynamical models. The accuracy of these forecasts is likely to improve as
283 the models are tested and developed further. However, in this paper we test the proposed
284 forecasting algorithm using observed SSTs. Such test describes an upper limit of the skill of the
285 proposed algorithm. The assessment of the same methodology using indices of SST forecasted by
286 global dynamical models will be addressed in future work.

287

288

289

Tables

290 **Table 1:** Summary of the coefficient of determination (R^2) between the average Nile flow from July to
 291 October and different combination of indices of ENSO and SIO.

Mode		ENSO	SIO	ENSO, SIO	Number of events (Observed Variance of Nile flow)
ENSO	SIO				
Neutral	Neutral	0.04	0.03	0.08	29 (6.76)
Neutral	Non-Neutral	0.05	0.28 ⁺	0.31 ⁺	26 (10.24)
Non-Neutral	Neutral	0.4 ⁺	0.02	0.43 ⁺	26 (5.8)
Non-Neutral	Non-Neutral	0.64 ⁺	0.6 ⁺	0.84 ⁺	19 (12.3)

292 Note: The values between brackets are for the observed variance of Nile flow of each mode in units of
 293 ($\text{MCM}^2/\text{day}^2$)

294 SIO: South Indian Ocean SSTs index, ENSO: ENSO index.

295 *Values that are significant at 5% significance level

296 ⁺ Values that are significant at 1% significance level

297

298

299

300

301

302

303 **Table 2:** Comparison between regions in the Indian Ocean used in ElDaw et al., 2003 and this

304 study to predict the Nile flow.

Region	Location	Study
1	(35°-44 ° S, 115 ° -130 ° E)	ElDaw et al, 2003
2	(0°-7 ° S, 90 ° -130 ° E)	
3	(35°-44 ° S, 20 ° -60 ° E)	
4	(10°-20 ° S, 110 ° -125 ° E)	
5	(50°E-80°E and 25°S-35°S)	This study

305

306 **Table 3:** Conditional probability of the Nile flow given SIO conditions

		Nile flow		
		High	Normal	Low
SIO	Warm	0	0.25	0.75
	Normal	0.23	0.39	0.39
	Cold	0.57	0.26	0.17

307

308

309

310

311

312 **Table 4:** Conditional probability of the Nile flow given ENSO conditions

		Nile flow		
		High	Normal	Low
ENSO	Warm	0.15	0.31	0.54
	Normal	0.22	0.38	0.41
	Cold	0.68	0.32	0

313

314

315 **Table 5:** Conditional probability of the Nile flow given SIO and ENSO conditions

SIO	Nile flow	ENSO		
		Warm	Normal	Cold
SIO Warm	High	0	0	0
	Normal	0.15	0.22	1
	Low	0.85	0.78	0
SIO Normal	High	0.1	0.14	0.57
	Normal	0.31	0.4	0.43
	Low	0.59	0.46	0
SIO Cold	High	0.33	0.42	0.83
	Normal	0.29	0.33	0.17
	Low	0.37	0.25	0

316

317

318

320 **Table 1:** Summary of some available forecast models of the Sea Surface Temperature

Model	Type of Model	Agency	Domain	Lead time up to (Months)	Resolution (km)	Reference
NCEP-CFS V2	Dynamical	National Centers for Environmental Prediction (NCEP)	Global	8	200	Saha et al., 2010
NASA-GMAO	Dynamical	NASA Goddard Space Flight Center- Global Modeling and Assimilation Office	Global	12	200	Bacmeister et al., 2000
ECMWF-System 4	Dynamical	European Centre for Medium-Range Weather Forecasts	Global	4	70	Molteni et al., 2011
UKMO-GCM	Dynamical	United Kingdom Met Office	Global	6	150	Graham et al., 2005
NOAA-CDC	Statistical	National Oceanic and Atmospheric Administration-Climate Diagnostic Center	Global	12	--	Pneland et al., 1998
CPC-Markov	Statistical	National Centers for Environmental Prediction-Climate Prediction Center	Nino 3 and Nino 3.4	8	--	Xue et al., 2000

REFERENCES

322
323
324
325
326
327
328
329
330
331
332
333
334
335
336
337
338
339
340
341

1. Abtew, W., Melesse, A. M. and Dessalegne, T. (2009), El Niño Southern Oscillation link to the Blue Nile River Basin hydrology. *Hydrol. Process.*, 23: 3653–3660. doi: 10.1002/hyp.7367
2. Amarasekera, K. N., Lee, R. F., Williams, E. R., and Eltahir, E. A. B: ENSO and the natural variability in the flow of tropical rivers, *J. Hydrol.*, 200, 24–39, 1996.
3. Beltrando, G., and Camberlin, P., 1993: Interannual variability of rainfall in Eastern Horn of Africa and indicators of atmospheric circulation. *International Journal of climatology* 13, 533-546.
4. Bacmeister, J. T., P. J. Pegion, S. D. Schubert, and M. J. Suarez, 2000: Atlas of seasonal means simulated by the NSIPP1 atmospheric GCM, NASA Tech. Memo-2000-104606, Vol. 17, 194pp.
5. Black E., J. Slingo, and K.R. Sperber, 2003: An observational study of the relationship between excessively strong short rains in coastal East Africa and Indian Ocean SST. *Mon. Wea. Rev.*, 31, 74-94.

- 342 6. Camberlin P., 1995. June-September rainfall in North-Eastern Africa and
343 atmospheric signals over the tropics: a zonal perspective. *International Journal of*
344 *Climatology* 15: 773-783.
- 345
- 346 7. Camberlin, Pierre, 1997: Rainfall Anomalies in the Source Region of the Nile and
347 Their Connection with the Indian Summer Monsoon. *J. Climate*, 10, 1380–1392.
- 348
- 349 8. Conway, D., and M. Hulme, 1993: Recent Fluctuations in precipitation and runoff
350 over the Nile subbasins and their impact on Main Nile discharge. *Climatic Change*,
351 25, 127 -151.
- 352
- 353 9. ElDaw, A., J. D. Salas, and L. A. Garcia, 2003: Long Range Forecasting of the Nile
354 River Flows Using Climate Forcing. *J. Applied Meteorology*, 42:890-904.
- 355
- 356 10. Eltahir, E. A. B., 1996: ElNino and the natural variability in the flow of the Nile
357 river. *Water Resour. Res.*, 32(1): 131-137.
- 358
- 359 11. Hastenrath, Stefan, Dierk Polzin, and Charles Mutai, 2011: Circulation Mechanisms
360 of Kenya Rainfall Anomalies. *J. Climate*, 24, 404–412.
- 361 12. Ju, J., and J. M. Slingo, 1995: The Asian summer monsoon and ENSO. *Quart. J. Roy.*
362 *Meteor. Soc.*, 121, 1133–1168.
- 363

- 364 13. Kawamura, R., 1998: A possible mechanism of the Asian summer monsoon-ENSO
365 coupling. *J. Meteor. Soc. Japan*, 76, 1009–1027.
366
- 367 14. Melesse, A., Abtew, W. Setegn, S.G., Desalegn, T. (2011). Hydrological Variability
368 and Climate of the Upper Blue Nile River Basin. In *Nile River Basin: Hydrology,*
369 *Climate and Water Use*. Springer. Melesse, Assefa M. (Ed.), 1st Edition., 2011, X,
370 480 p. 200 illus, Part 1, 3-37, DOI: 10.1007/978-94-007-0689-7_1
371
- 372 15. Molteni, F., T. Stockdale, M. Balmaseda, G. Balsamo, R. Buizza, L. Ferranti, L.
373 Magnusson, K. Mogensen, T. Palmer & F. Vitart, 2011: The new ECMWF seasonal
374 forecast system (System 4). ECMWF Research Department Technical
375 Memorandum n.656, ECMWF, Shinfield Park, Reading RG2-9AX, UK, pp. 51.
376
- 377 16. ElSanabary, M. H., Gan, T. Y., Mwale, D., 204: Application of wavelet empirical
378 orthogonal function analysis to investigate the nonstationary character of Ethiopian
379 rainfall and its teleconnection to nonstationary global Sea Surface Temperature
380 variations for 1900-1998. *International Journal of Climatology*.
381 DOI:10.1002/joc.3802
382
- 383 17. Graham. R., M. Gordon, P.J. McLean, S. Ineson, M.R. Huddleston, M.K. Davey, A.
384 Brookshaw, R.T.H. Barnes, 2005: A performance comparison of coupled and
385 uncoupled versions of the Met Office seasonal prediction general circulation
386 model. *Tellus*, 57A, 320-339.
387

- 388 18. Giro, D. Grimes, D., Black, E. 2011: Teleconnections between Ethiopian summer
389 rainfall and sea surface temperature: part I Observation and Modeling. *Climate*
390 *Dynamics* 37:103-199.
- 391
392 19. Gissila, T., Black, E., Grimes, D. I. F., Slingo, J.M 2004: Seasonal forecasting of the
393 Ethiopian Summer rains. *International Journal of Climatology* 24: 1345-1358.
- 394
- 395 20. Penland, C. and L. Matrosova, 1998: Prediction of Tropical Atlantic Sea Surface
396 Temperatures Using Linear Inverse Modeling. *J. Climate*, 11, 483-496.
- 397
- 398 21. Saha, Suranjana, and Coauthors, 2010: The NCEP Climate Forecast System
399 Reanalysis. *Bull. Amer. Meteor. Soc.*, 91, 1015.1057. doi:
400 10.1175/2010BAMS3001.1.
- 401
- 402 22. Suranjana Saha, Shrinivas Moorthi, Xingren Wu, Jiande Wang, Sudhir Nadiga,
403 Patrick Tripp, Hua-Lu Pan, David Behringer, Yu-Tai Hou, Hui-ya Chuang, Mark
404 Iredell, Michael Ek, Jesse Meng, Rongqian Yang, Huug van den Dool, Qin Zhang,
405 Wanqiu Wang, Mingyue Chen, 2013 : The NCEP Climate Forecast System
406 Version 2. (*Journal of Climate*, under review.)
- 407
- 408 23. Shukla, J., and J. M. Wallace, 1983: Numerical simulation of the atmospheric
409 response to equatorial Pacific sea surface temperature anomalies. *J. Atmos. Sci.*, 40,
410 1613–1630.

411
412
413
414
415
416
417
418
419
420
421
422
423
424
425
426
427
428
429
430
431
432
433

24. Siam, M. S., Wang, G., Estelle, ME., and Eltahir, E. A. B, 2014: Role of the Indian Ocean Sea Surface Temperature in shaping natural variability in the flow of the Nile River. *Climate Dynamics*, in press.

25. Soman, M. K., and J. Slingo, 1997: Sensitivity of the Asian summer monsoon to aspects of sea-surface-temperature anomalies in the tropical pacific ocean. *Q. J. R. Meteorol. Soc.*, 123, 309-336.

26. Trenberth, K. E., 1997: The Definition of El Niño. *Bulletin of the American Meteorological Society*, 78, 2771-2777.

27. Wang, G., and Eltahir E. A. B, 1999: Use of ENSO information in Medium and Long Range Forecasting of the Nile Floods . *J. Climate*, 12, 1726-1737.

28. West, M., 1989: *Bayesian Forecasting and Dynamic Models*. Springer, 704 pp.

29. Winkler, R., 1972: *An introduction to Bayesian inference and Decision*. Holt, Rinchart and Winstoon, 563 pp.

30. Xue, Y., A. Leetmaa, and M. Ji, 2000: ENSO prediction with Markov model: The impact of sea level. *J. Climate*, 13, 849-871.

434 31. Yang, J. L., Q. Y. Liu, S. P. Xie, et al., 2007: Impact of the Indian Ocean SST basin
435 mode on the Asian summer monsoon, *Geophys. Res. Lett.*, 34, L02708,
436 doi:10.1029/2006GL028571.

437

438

439

440

441

442

443

444

445

446

447

448

449

450

451

452

453

454

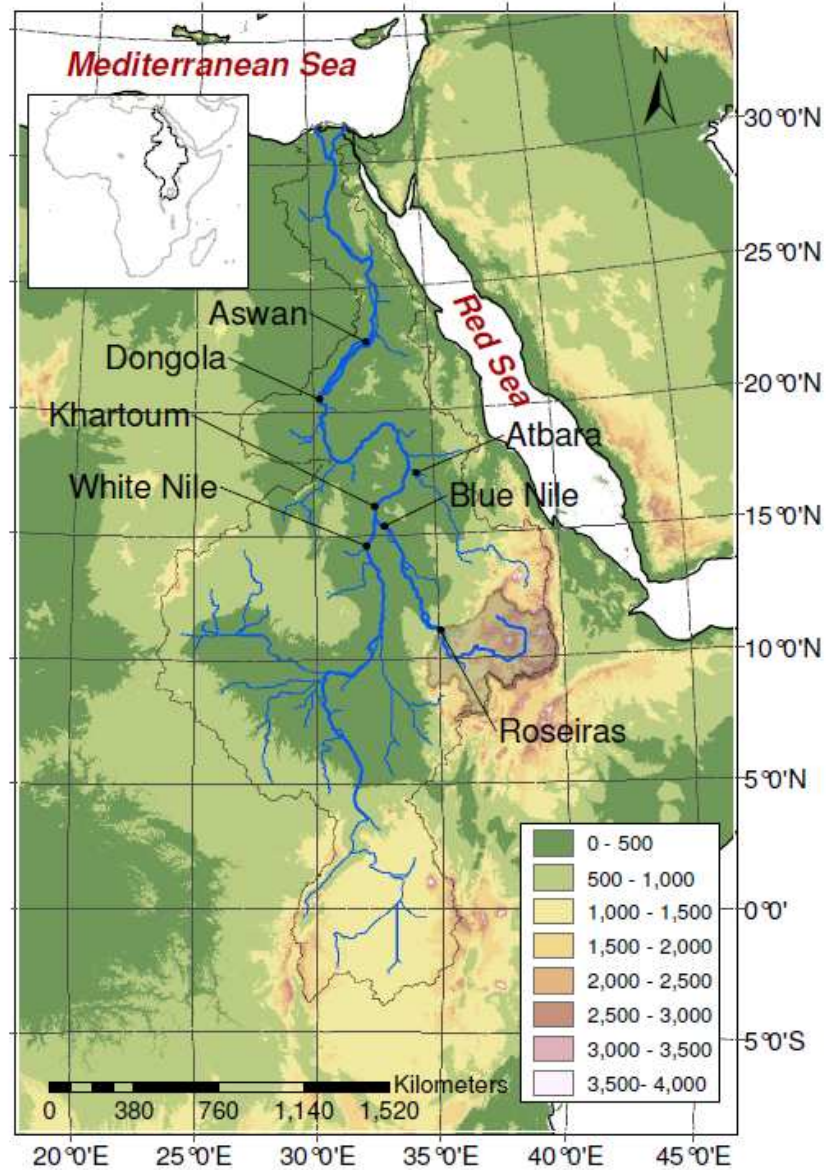
455

456

Figures

457

458



459

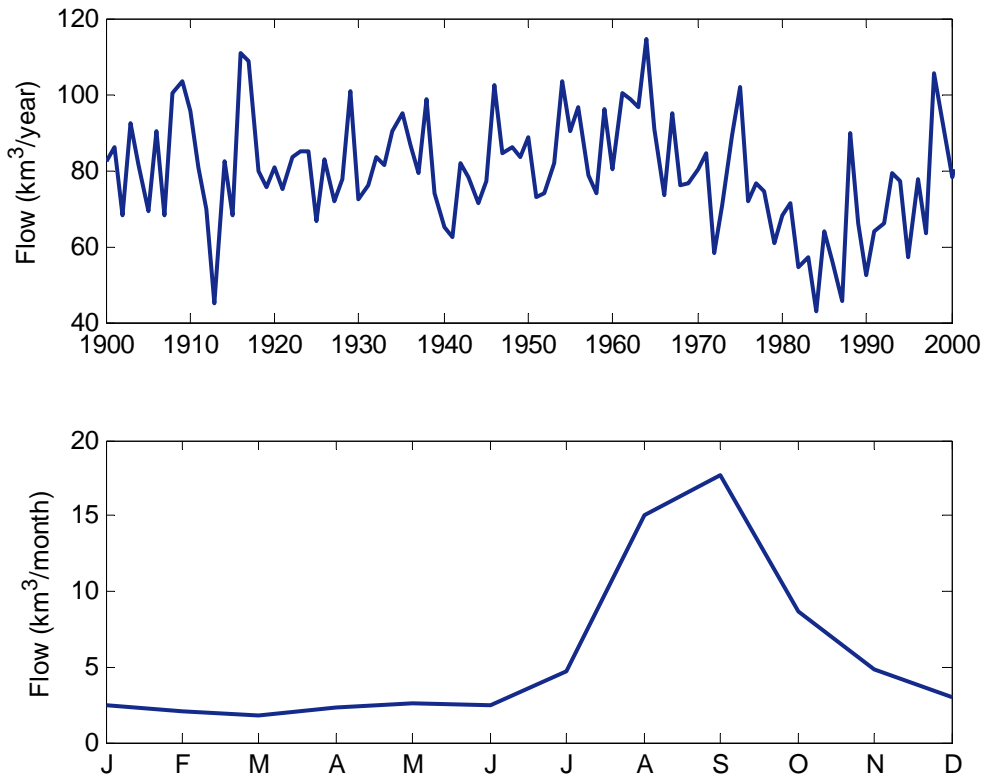
460

461 **Figure 1:** Topographic map of the Nile basin showing the outlet of the Upper Blue Nile basin (shaded in
462 gray) at Roseiras. The White and Blue Nile join together at Khartoum the form the main branch of the Nile
463 that flows directly to Dongola in the North.

464

465

466



480 **Figure 2:** Annual Nile flow (Top) and seasonal cycle (Bottom) of the flow at Dongola for the period from
481 1900 to 2000.

482

483

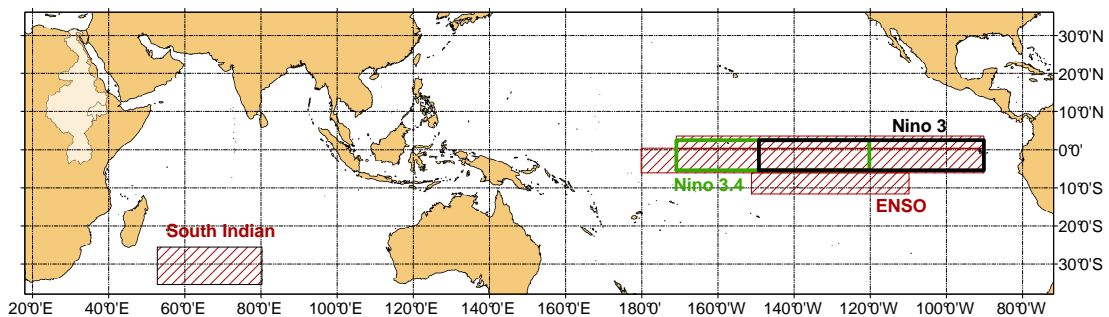
484

485

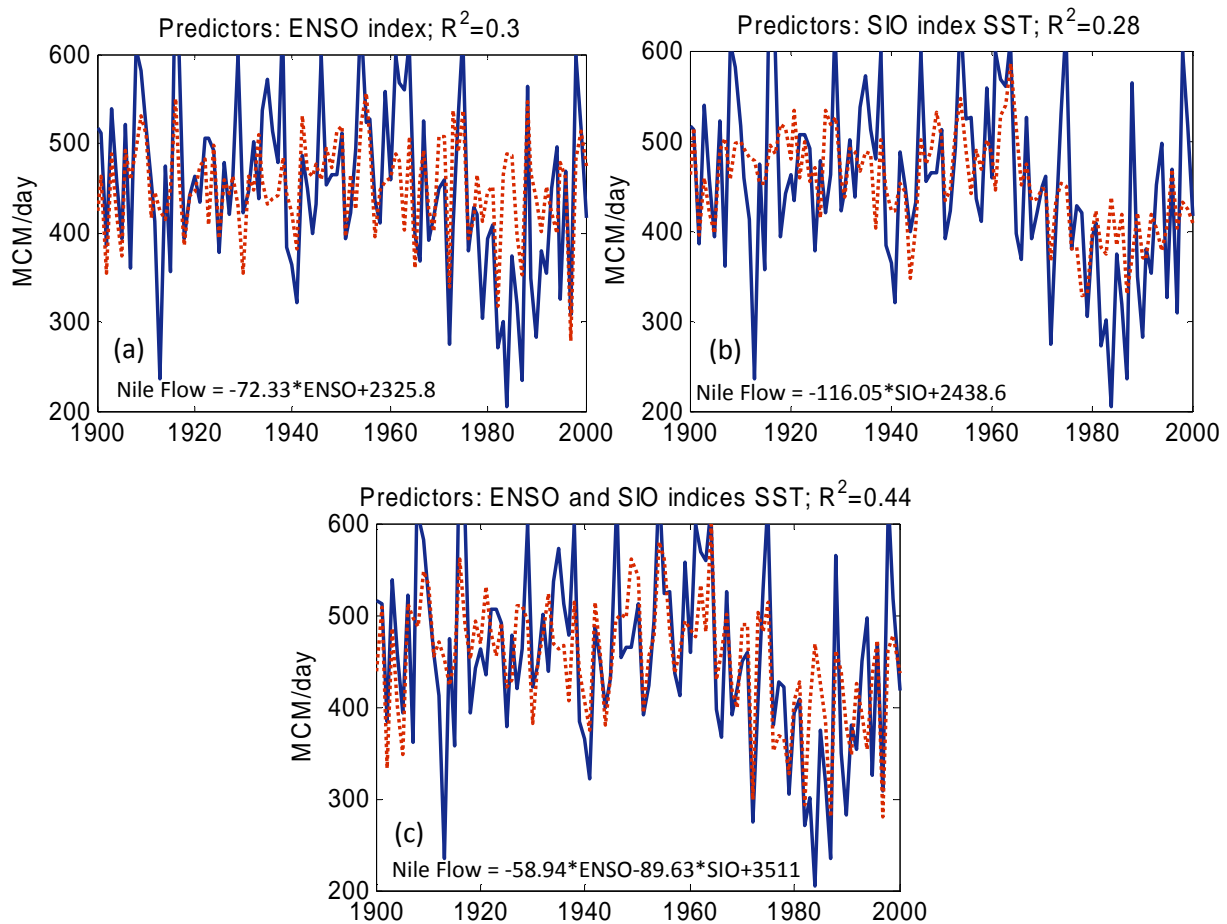
486

487

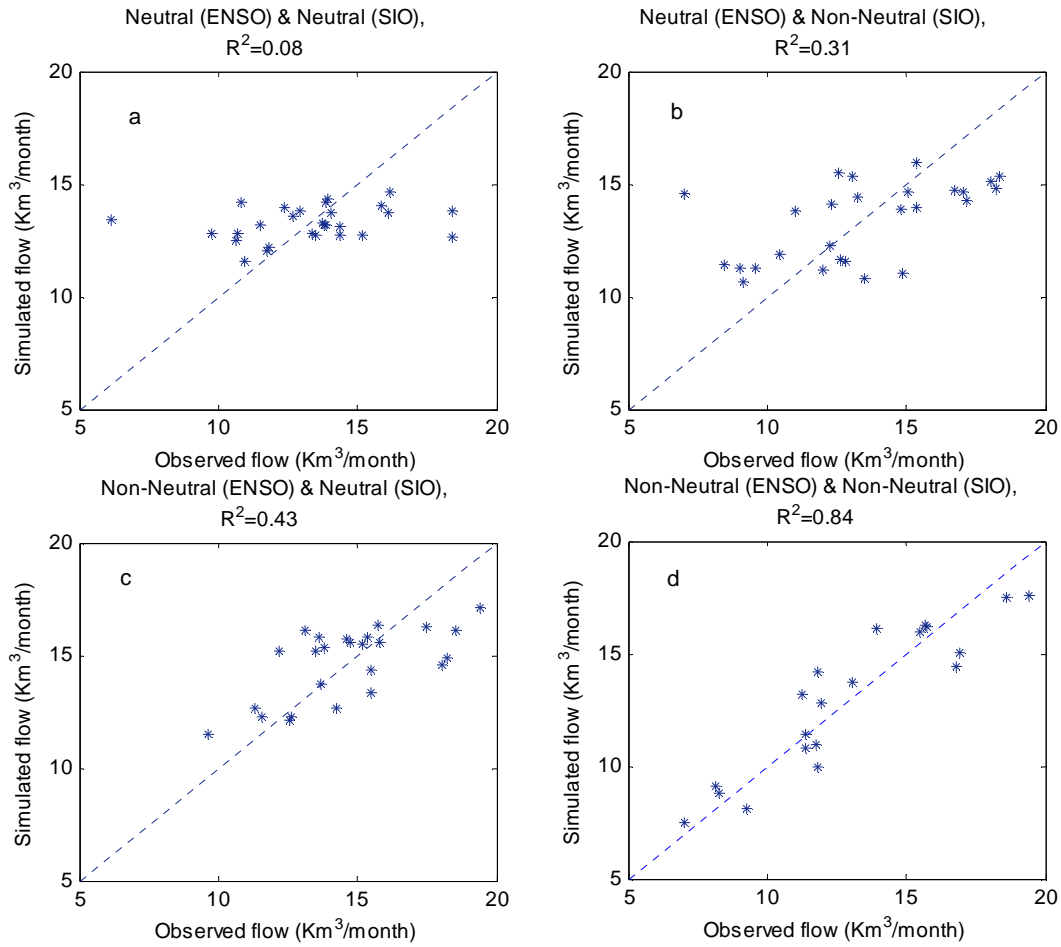
488



489 **Figure 3:** World map showing areas that cover the ENSO and North and South Indian Ocean SSTs indices.
490 The Nino 3 and 3.4 are outlined in black and green respectively. The whole Nile basin is outlined in black.



493 **Figure 4:** Observed (Solid Blue lines) and simulated (Dashed Red lines) average Nile flows in Million
 494 Cubic Meter per day (MCM/day) from July to October at Dongola using: a) ENSO index, b) SIO index and
 495 c) ENSO and SIO indices as predictors for the period 1900 to 2000. The simulated flows are calculated
 496 based on the equations shown in each figure, in which the predictands are the average observed SSTs
 497 over the ENSO and SIO regions in degrees Celsius and the predictor is the average Nile flow from July to
 498 October in Million Cubic Meter per day (MCM/day).



503

504 **Figure 5:** A comparison between the observed and simulated Nile flow showing the different modes of
 505 variability for the period from 1900 to 2000: a) Neutral ENSO (29 events) and SIO, b) Neutral ENSO and
 506 Non-Neutral SSTs in SIO (26 events), c) Non-Neutral ENSO and Neutral SSTs in SIO (26 events) and finally,
 507 d) Non-Neutral ENSO and Non-Neutral SSTs in SIO (19 events).

508

509

510

511

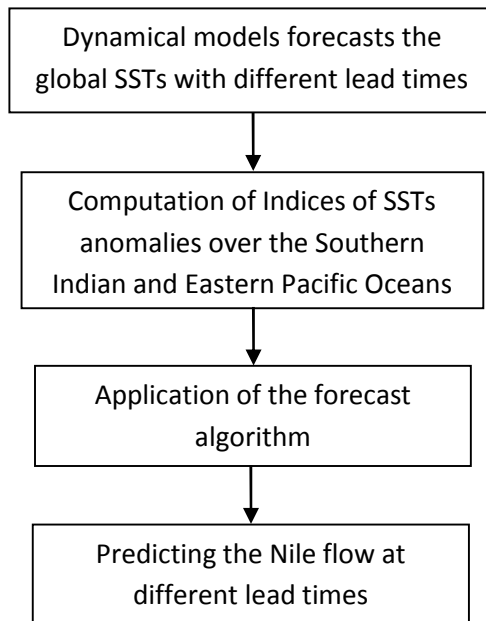
512

513

514

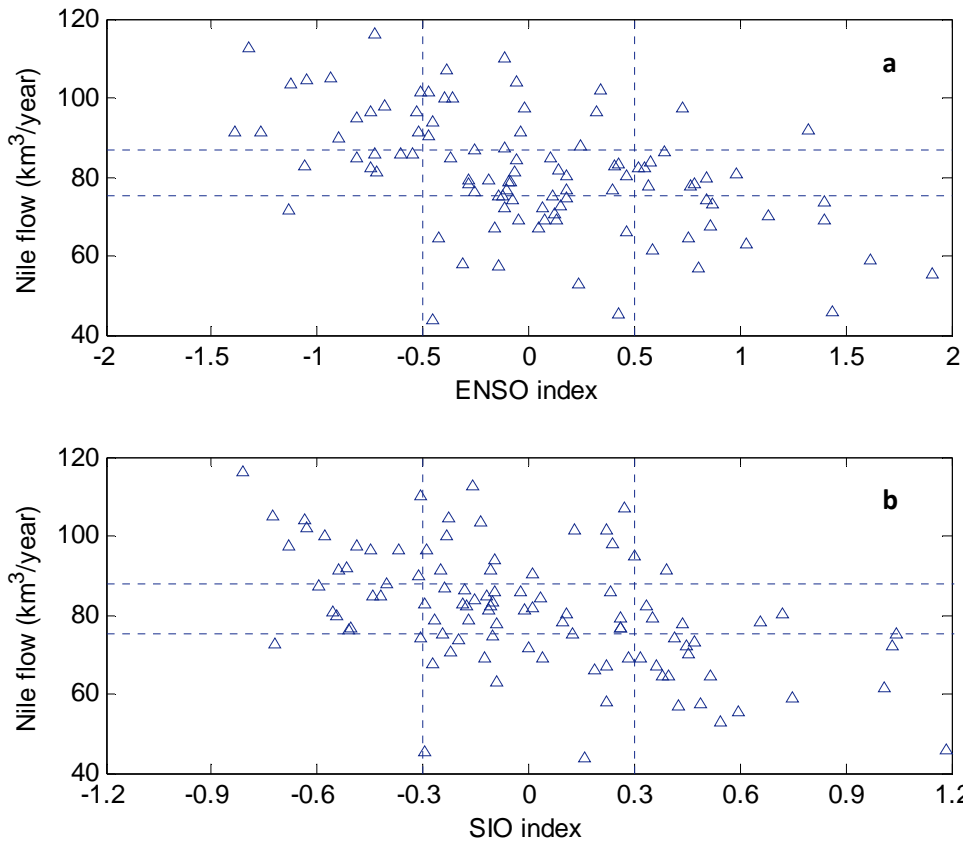
515

516
517
518
519
520
521
522
523
524
525
526



527 **Figure 6:** Schematic of the hybrid methodology for predicting the Nile flow using the SSTs forecasts of
528 the dynamical models and the proposed forecast algorithm.

529
530
531
532



533

534 **Figure 7:** Relations between the annual Nile flow and different indices for the period (1900-2000): a)
 535 ENSO, and b) SIO. The horizontal lines represent the boundaries for the “high”, “normal” and “low”
 536 categories of the annual flow. The vertical lines represent the boundaries for the “Warm”, “normal”, and
 537 “cold” conditions for ENSO and SIO indices.

538

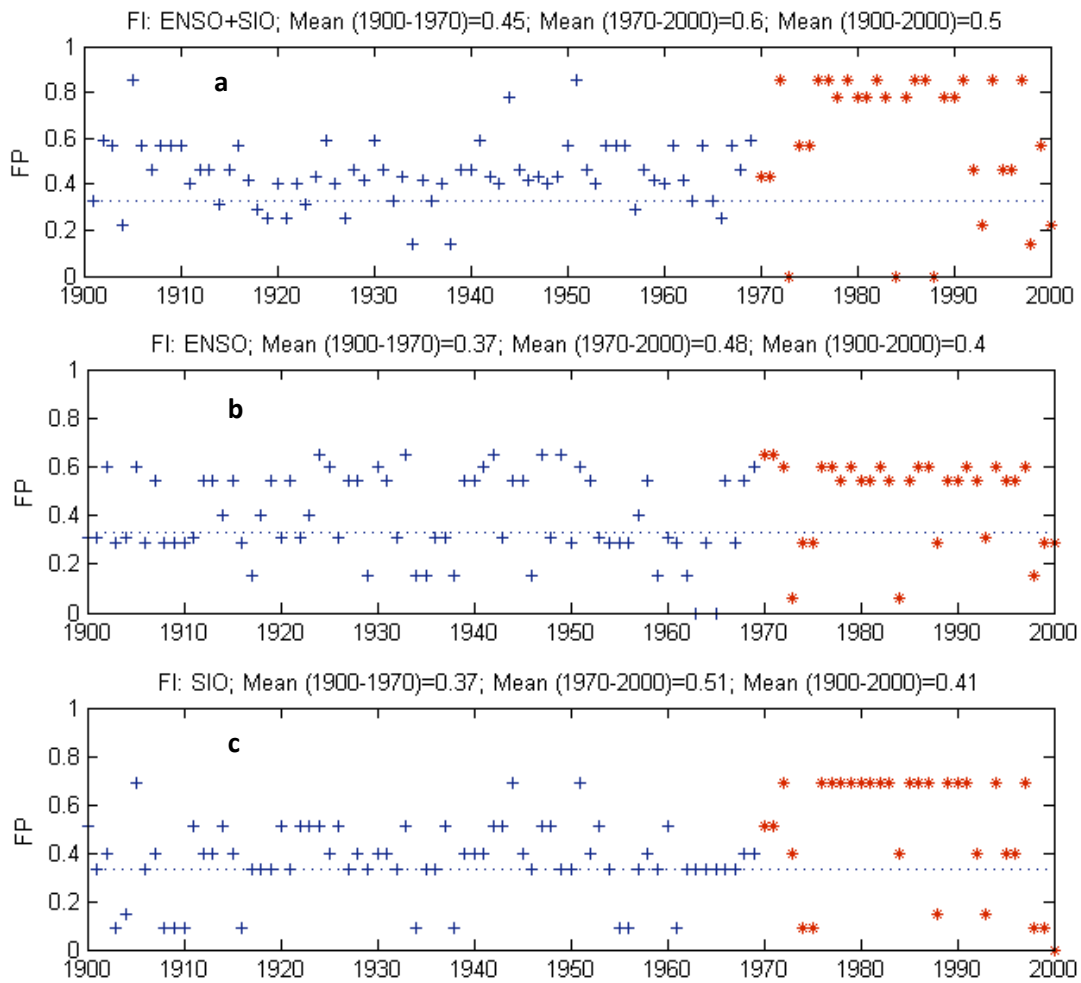
539

540

541

542

543



544

545 **Figure 8:** Time series of the forecast probability using different indices: a) ENSO and SIO together, b)
 546 ENSO, and c) SIO. The period (1900-1970) is used for calculating the probabilities (shown in crosses)
 547 using Eq. (2) and (1970-2000) for validation (shown in stars).

548